Journal of Non-Crystalline Solids 585 (2022) 121544

Contents lists available at ScienceDirect

Journal of Non-Crystalline Solids

journal homepage: www.elsevier.com/locate/jnoncrysol

Effect of Nb and Al on *in vitro* dissolution behavior and structure of Na_2O-MgO—CaO-P_2O_5 glasses

Natalia Anna Wójcik [a,*], Stefania Wolff [a], Jakub Lech Karczewski [a], Małgorzata Rutkowska [b], Sharafat Ali [c]

[a] Advanced Materials Center, Institute of Nanotechnology and Materials Engeenering, Gdańsk University of Technology, 11/12G. Narutowicza Street, Gdańsk 80-233, Poland
[b] Department of Analytical Chemistry, Faculty of Chemistry, Gdańsk University of Technology, 11/12G. Narutowicza Street, Gdańsk 80-233, Poland
[c] Department of Built Environment and Energy Technology, Linnaeus University, Växjö 35195, Sweden

ARTICLE INFO

Keywords:
Na-Mg-Ca-Al-Nb-P-O glass
In vitro dissolution
FTIR
Thermal properties

ABSTRACT

In vitro dissolution, structure, and thermal properties of the glass series Na_2O-MgO—CaO—Nb_2O_5 -Al_2O_3-P_2O_5 were studied. The dissolution behavior in phosphate-buffered saline (PBS) confirmed the potential bioactive properties of tested glasses. The dissolution process was found to depend on the Al, Nb, and Mg contents. Al, respectively, suppresses the Nb and accelerates the Mg release process from the glasses. Moreover, Al stays highly bonded in the phosphate network during 14 days of immersion. In all glasses, the phosphate network was found to be highly disrupted and built mostly of Q^1 units. Al and Mg addition decreases the polymerization of the glass network. The Nb addition effect was found to be the opposite. Thermal properties were correlated mostly with the Nb and Al contents. However, the fragility index of glasses increases with the content of P and Al.

1. Introduction

Na_2O—CaO-P_2O_5 glasses are well-known as bioactive glasses with potential application for bone implants [1–3]. Low melting temperature and faster dissolution in aqueous solutions; give these Na_2O—CaO-P_2O_5 glasses the opportunity to be good competitors to well-known and already in use silicate-bioglasses [4,5]. Moreover, a high tendency to crystallize during thermal processing makes most bioglasses less suitable, resulting in a reduction in dissolution rate and bioactivity [6,7]. On the other hand, the excessive dissolution rate of phosphate glasses may also be a disadvantage for bone implants, which required suitable long-time stability needed to repair bone defects. The thermal properties and chemical durability of bioglasses can be significantly improved by doping with niobium oxide [7–9]. The niobate units act as an intermediate glass former in the phosphate glass network and therefore its thermal properties can be controlled by the addition of Nb_2O_5 [10]. Additionally, niobium exhibits lower cytotoxicity than other metal ions [11] and can have a major impact on bone regenerative properties [12,13]. A. Obata et al. reported that it can stimulate mineralization in human osteoblast populations [14]. While the small addition (up to 1 mol%) of Nb_2O_5 to 45S5 (45 wt% SiO_2, 24.5 wt% CaO, 24.5 wt% Na_2O, 6.0 wt% P_2O_5) bioglass allows to characterize them as having angiogenic potential [15]. In our previous paper, we have shown that the addition of niobium slightly reduces the *in vitro* dissolution of Na-Ca-P-Si-O glasses however the formation of the HAp layer was not disrupted [6]. For the phosphate-based glasses, Nb_2O_5 addition was found to improve bioactive properties [16]. It was also reported that niobate released from the glass during immersion in simulated body fluid (SBF) while in glass-ceramic it stayed highly bonded [8].

The incorporation of MgO also influences the thermal properties and dissolution rate of phosphate bioglasses [5]. The magnesium addition shown to increase the glass transition temperature of phosphate glass caused by the high field strength of Mg^{2+} ions and the thermal stability by suppressing its crystallization process [17–22]. The biodegradability studies of Na_2O–MgO–CaO–P_2O_5 glasses confirmed that the increase in MgO content decreased the glass dissolution rate [23]. However, in our recent paper [5] we have reported the inverse correlation. The increase in magnesium concentration was found to enhance the biosolubility of Na_2O—CaO-Al_2O_3-P_2O_5 glasses by increasing their dissolution rate and supporting the formation of CaP-rich layers on the surface.

Currently, the effect of the Al_2O_3 crucible material on phosphate glass composition, structure, and properties has attracted increasing

* Corresponding author.
E-mail address: natalia.wojcik@pg.edu.pl (N.A. Wójcik).

https://doi.org/10.1016/j.jnoncrysol.2022.121544
Received 4 January 2022; Received in revised form 28 February 2022; Accepted 1 March 2022
Available online 9 March 2022

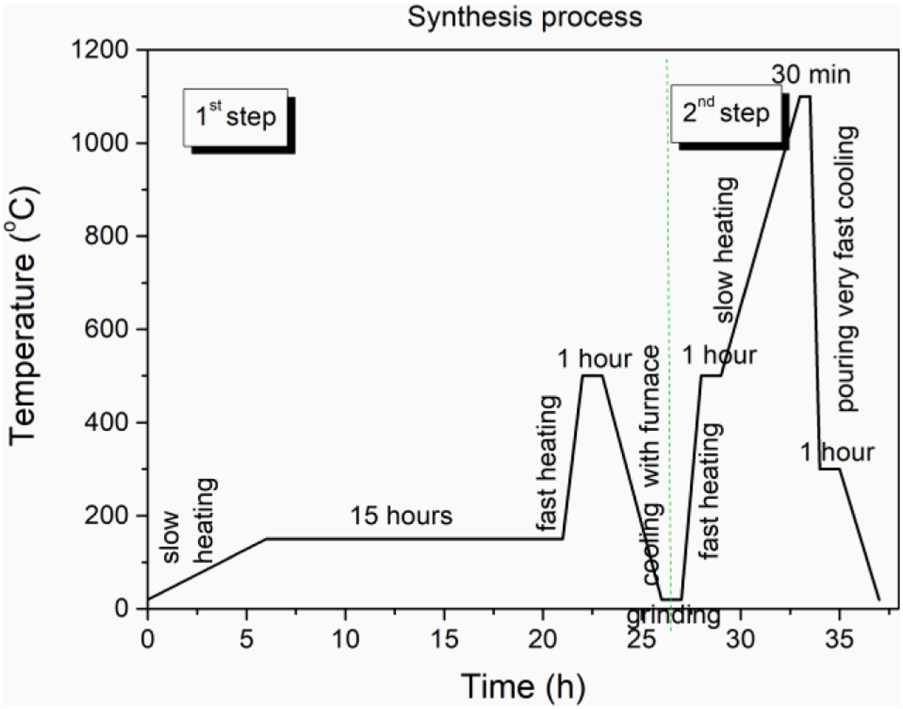

Fig. 1. Glass synthesis route followed for Na_2O -MgO- CaO - P_2O_5 - Al_2O_3 -Nb_2O_5 glasses.

attention in glass science. Moreover, there is also growing interest in the effect of Al_2O_3 on *in vitro* bioactivity of bioglasses [24–26]. It was found that doping with Al_2O_3 (up to 1.5 mol%) had no strong effect on the bioactive properties of silicate-based bio-glasses but improved their long-term stability [27]. In the case of sodium-calcium-phosphate bio-glasses the addition of Al_2O_3 (up to 1.9 mol%), increased the formation of hydroxyl carbonate apatite layer on the surface of the immersed glass in simulated body fluid [24]. However, the weight loss of the glass was also reduced with the incorporation of only 3 mol% of Al_2O_3 while the doping with $Al_2O_3 \geq 5$ mol% negatively affects the bioactivity of the Na_2O–CaO–P_2O_5 glasses [25]. The addition of Al_2O_3 can also improve the thermal properties of phosphate bioglasses [3].

There are few studies about the separate effect of Nb, Al, and Mg on the *in vitro* dissolution of calcium-phosphate invert glasses and there is still a lack of knowledge about their combined effect. Therefore, this work aims to fill this gap. In this work, we presented the mixed impact of Nb, Al, and Mg on the structure, thermal properties, and *in vitro* dissolution of calcium-phosphate glasses.

2. Materials and methods

1.1. Glass preparation

Sodium-calcium-phosphate glass system doped with up to 10 mol% of MgO and/or Nb_2O_5 was synthesized using the traditional melt quenching technique. The starting composition of samples was 16 Na_2O - (10-x) MgO- 38 CaO - xNb_2O_5 - 36 P_2O_5 (in mol%), where the contents of dopants change between 0, 3, 5, 7, and 10 mol%. The reagents: Na_2HPO_4 (Acros 99%), NH_6PO_4 (Chempur pure p.a.), $CaCO_3$ (Sigma-Aldrich >99.95%), Nb_2O_5 (Alfa Aesar 99.5%), and MgO (Chempur p.a.) were mixed in an agate mortar to obtain homogenous powders. The melting was conducted in an Al_2O_3 crucible, generally, the aluminum crucible react with the melt particularly containing phosphorous. Al_2O_3 leached from the crucible was considered as a source of Al_2O_3 in the glass. The glass synthesis process was divided into two parts. During the first one, ~30 g of powders were slowly heated up to a temperature of 150 °C and next to 500 °C to evaporate ammonia from reagents. During heating, the foam of powders and ammonia came out from the crucible and stayed on the walls of the crucibles. After cooling with the furnace, the sintered powders were taken out from crucibles and grinded once again in an agate mortar. In the second step of the glass synthesis process, the already sintered powder was heated up to 1100 °C and held at this temperature for about 30 min, in an air atmosphere. Some samples were still highly reactive during second heating and additional grinding was needed. The melts were poured onto a preheated brass plate and stamped. After one hour, samples were cooled to room temperature. A detailed description of the melting process with heating/cooling times and temperatures is shown in Fig. 1.

1.2. Compositional analysis and structure characterization

The topography and compositions of glass samples were studied using Energy Dispersive X-ray Spectrometer (EDX GENESIS Apex Apollo X60 Spectrometer) and Scanning Electron Microscope (SEM), FEI Company Quanta FEG250. The measurements were conducted on freshly fractured samples and at least on 3 different areas for each sample. All EDX values are given with an accuracy of around ± 5% standard deviation.

The structure of glasses was studied with IR spectroscopy. Powdered samples were mixed with KBr powder and pressed using a hydraulic press to obtain plane-parallel plates. Measurements were done using a Frontier FTIR spectrometer (PerkinElmer). The IR spectra were scanned 64 times for each sample in the range of 400–4000 cm^{-1} with a resolution of 4 cm^{-1}. The IR spectra were also background-corrected only in the range of 400–800 cm^{-1} and normalized to the dominating band at ~1100 cm^{-1}. The bands' positions were estimated using the Origin software and with precise ± 2 cm^{-1}.

1.3. In vitro dissolution in PBS

The *in vitro* dissolution process was studied in phosphate-buffered saline solution (PBS) under static conditions. The PBS (Fisher Bio-Reagents) solution (0.01 M phosphate buffer, 0.0027 M potassium chloride, and 0.137 M sodium chloride) was prepared by dissolving

Table 1
IDs and obtained compositions of all samples.

Glass code	Starting composition(at%)	Final composition(at%)	EFCS($Å^{-2}$)
0Nb	$Na_{8.1}Mg_{2.4}Ca_{9.5}P_{18.3}O_{61.7}$	$Na_{6.9}Mg_{1.8}Ca_{10}Al_3P_{16.7}O_{61.6}$	2.28
0.8Nb	$Na_{7.7}Mg_{2.2}Ca_{9.1}Nb_{1.4}P_{17.5}O_{62.2}$	$Na_{8.7}Mg_{1.8}Ca_{8.1}Nb_{0.8}Al_{3.8}P_{15.6}O_{61.1}$	2.55
1.4Nb	$Na_{7.5}Mg_{1.5}Ca_{8.9}Nb_{2.2}P_{17.1}O_{62.6}$	$Na_{6.9}Mg_{0.8}Ca_{9.4}Nb_{1.4}Al_{0.8}P_{17.7}O_{62.9}$	2.18
1.8Nb	$Na_{7.4}Mg_{0.9}Ca_{8.8}Nb_3P_{16.8}O_{63.1}$	$Na_{5.5}Mg_{0.3}Ca_{10.1.4}Nb_{1.8}Al_{2.7}P_{16.4}O_{63}$	2.72
3.4Nb	$Na_{7.2}Ca_{8.2.2Nb4.3}P_{16.4}O_{63.7}$	$Na_7Ca_9Nb_{3.4}Al_{0.8}P_{16.5}O_{63.4}$	2.69
Experimental uncertainties		± 5%	± 0.01

tablet in 200 ml deionized water. The PBS has a pH of 7.4 at a temperature of 20 °C before starting the tests. For static dissolution studies, 0.3 g of samples were put in 20 ml of PBS and placed in an incubating orbital shaker Labnet 311DS (at ambient atmosphere) with a rotation speed of 120 rpm and temperature of 36.6 °C. The *in vitro* measurements were performed parallel for two pieces of each sample for each endpoint, *i.e.*, 7 and 14 days. Before the test, the top layers of samples were slightly polished with grinding paper to improve the adhesion of depositing calcium phosphates. After immersion, the samples were rinsed in the deionized water and dried in a desiccator for 24 h.

The total percentage change in weight was calculated based on the mass before and after the immersion in PBS. The morphology of the top layers of the samples was examined with SEM. SEM observations were done with a SE-ETD detector (secondary electron—Everhart-Thornley detector) using a 20 kV beam accelerating voltage and under a high vacuum (pressure 10^{-4} Pa). The composition of the glass surface was checked by EDX analysis.

The pH of the PBS solution was measured at several immersion times to obtain information on the pH trends and understand the dissolution behavior. Also, 3 consecutive pH measurement points were applied to check the differences between every consecutive measurement. The mean value of all obtained results for each composition was taken as the representative one. Calibration of the pH meter (Elmetron CPC-411) was carried out using three different pH standards (pH 4, 7, and 9). The procedure yielded an of ± 0.01.

After 7 and 14 days of immersion, the PBS solutions were analyzed using atomic emission spectrometry with microwave plasma atomization (MP-AES 4210 by Agilent) to determine concentrations of selected elements, *e.g.*, Ca, Na, Mg, P, Nb, and Al. Ca, Mg, P, and Al standard solutions were obtained from Sigma-Aldrich (Germany). Nb standard solution was obtained from Sigma-Aldrich (Canada). Na standard solution was purchased from Ms Spectrum (Poland). The determination of the elements in the tested samples was carried out at specific wavelengths for each element. The uncertainties of determining concentrations are below 2%.

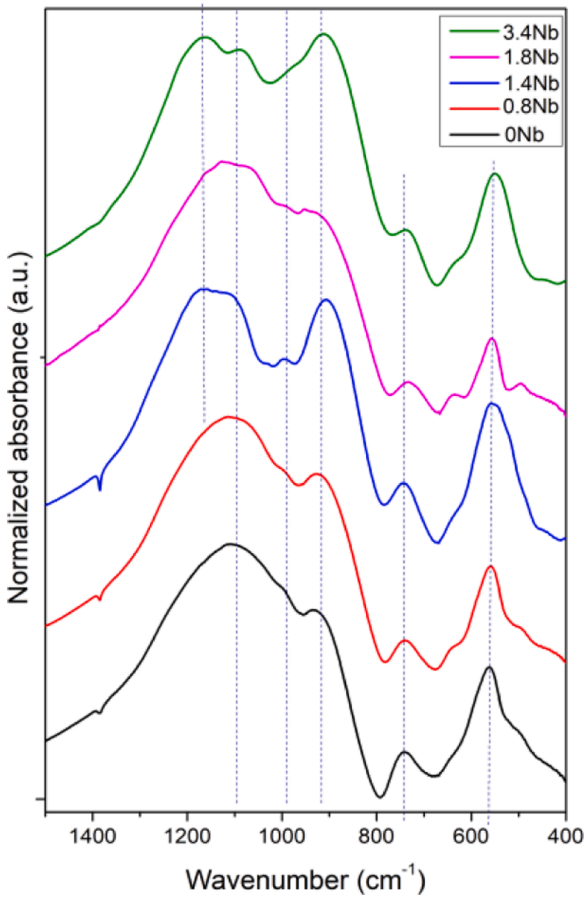

Fig. 3. FTIR spectra for all as-quenched samples. Spectra have been background corrected and offset by the maximum value of IR intensity obtained in the range of 400 – 1500 cm^{-1}, to allow better comparison.

Fig. 2. Photograph of the as-quenched samples: 0Nb, 0.8Nb, 1.4Nb, 1.8Nb, and 3.4Nb (from left to right).

1.4. Thermal properties

Glass transition temperatures (T_g) and heat capacity during the glass transition (C_p) as well as crystallization temperatures (T_{cr}) were measured on powdered samples placed in the Al_2O_3 crucibles, using differential scanning calorimetry (DSC) up to 1000 °C in flowing synthetic air with a Netzsch STA 449 F1 instrument and a heating rate of 20 °C min^{-1}. The glass transition temperature was estimated based on the onset of an endothermic drift on the DSC signal. The exothermic maxima found in all samples are assigned to crystallization processes. Proteus software provided by NETZSCH was used for the estimation of thermal properties parameters with the precision of ± 2 °C.

3. Results and discussion

3.1. The structure of glasses

Five samples having different contents of Nb, Al and Mg, were synthesized. The final compositions of obtained glasses are listed in Table 1. Samples doped with niobium oxide were of light greenish color whose intensity slightly increases with the niobium content as shown in Fig. 2. In all samples, Al_2O_3 was detected as it diffused into melts from crucible material. The content of Al was found to be high in samples: 0Nb, 0.8Nb, and 1.8Nb. Most probably, the reason is additional grinding during the final melting process, which was performed to obtain homogenous materials. Since the Al content differs in all samples, it gave us the opportunity to study its influence on glass structure and properties. The content of sodium was found to vary between 5.5 and 8.7 at% while the highest was observed for sample 1.4Nb which also showed the lowest content of Ca ~8.1 at% and the highest dissolution of Al up to 3.8 at%.

IR spectroscopy was used to check the glass structure. FTIR spectra are displayed in Fig. 3 for all glasses. It can be seen that all glasses showed the rounded shapes of curves bands indicating the amorphous nature. The FTIR bands observed for samples are mainly due to the phosphate network, which appears in the range 450–1500 cm^{-1} [28]. First, we will start with the glass 0Nb containing 1.8 at% of Mg and 3 at % of Al and no Nb. This sample has an O:P ratio close to 3.7, indicating a highly disrupted structure made mostly of Q^1 units and also with the presence of Q^0 units (Q^n denotes a phosphate tetrahedral unit with *n* bridging and *4-n* terminal oxygen atoms). The FTIR spectrum of the 0Nb sample shows main bands at ~1100 cm^{-1} and 915 cm^{-1} which are due to the asymmetric stretching mode of the chain-terminating Q^1 group ($_{vas}(PO_3)^{2-}$) and the asymmetric stretching vibration of P-O-P bridges of the Q^1 group ($_{vas}$(P-O-P)) [29–33]. Two small envelopes are visible at ~993 cm^{-1} and 746 cm^{-1} which are correlated with the asymmetric stretching vibration of the Q^0 unit ($_{vas}(PO_4)^{3-}$) and the symmetric stretching vibrations of P-O-P linkages ($_{vs}$(P-O-P)), respectively [34]. The highly pronounced band found at ~560 can be assigned to $_{\nu}$(P-O) bonding in $(PO_4)^{3-}$ [35]. The obtained FTIR results are in good agreement with the expected distribution of Q^1 and Q^0 units, calculated based on 0Nb glass stoichiometry. However, there is also one barely noticeable envelope at 490 cm^{-1} which is due to $_{\nu}$(O-P-O) in $(PO_2)^-$ modes and indicating the occurrence of Q^2 units in glass network [36]. which resulted from Q^1 site disproportionation reactions that occurred during the reorganization of the glass liquid $2Q^1 = Q^2 + Q^0$ [37]. The addition of 0.8 at% of Nb to composition only subtle changed glass structure. The FTIR spectrum of the 0.8Nb sample shows that the relative intensity of the envelope at ~915 cm^{-1} slightly increased suggesting the higher contribution of Q^1 units. This change indicates the slightly higher polymerized network in sample 0.8Nb than in sample 0Nb. It can be due to the different roles played by MgO and Nb_2O_5 in the phosphate glass network. The previous study has shown that the substitution of MgO for P_2O_5 increases the depolymerization of Na_2O-MgO—CaO-P_2O_5 glasses [38]. The opposite behavior was observed for Nb-doping, its effect on the phosphate network was manifested by the decrease in the content of the orthophosphate units (Q^0) and the parallel enhancement of the pyrophosphate units (Q^1) [39]. At the same time, in the FTIR spectrum of 0.8Nb, an additional small envelope occurred at ~633 cm^{-1} which is evidence of niobium incorporation into the glass structure. This envelope can be correlated with the asymmetric stretching vibration of the Nb-O-Nb bridges of distorted NbO_6 octahedra $_{vas}$(Nb-O) [36]. Sample 1.4Nb which contains a similar quantity of MgO and Nb_2O_5 has an O:P ratio of 3.6, suggesting a slightly higher polymerized network than the two just discussed samples. This structural difference is noticeable on its FTIR spectrum, which is dominated by bands at 1170, 1100, and 907 cm^{-1}. The newly observed band corresponds to the symmetric stretching vibration of the terminal PO_2^- groups, $_{vs}(PO_2^-)$, of Q^2 units. The appearance of this band as well as the significant increase in the relative intensity of the band at 997 cm^{-1} confirm the Nb role in the phosphate glass network. Therefore, the band at 997 cm^{-1} should be considered during the estimation of stoichiometric network polymerization. Since the O:(P+Nb) ratio of glass 1.4Nb is equal to 3.3, indicating the presence of Q^1 units as well as prominent content of Q^2 units in the network. However, this sample has also a significantly lower content of Al_2O_3 than the previous two. It is known that Al^{3+} ions have a great influence on the glass structure [40,41]. The Al^{3+} coordinates preferentially with terminal oxygen atoms of the PO_2^- and PO_3^{2-} groups and consequently reduce the relative population of terminal oxygen atoms. The formation of the P–O–Al–O–P bridging bonds provides strong cross-linking between phosphate chains [42]. This can be visible as the structural changes from metaphosphate (Q^2) and pyrophosphate structural units (Q^1) toward short isolated orthophosphate units (Q^0) form, while Al_2O_3 content reaches more than 6.5 at% in Na_2O—CaO-P_2O_5 glass [43]. The same tendency is also observed between our glass with a trace amount of Al (0.8 at%) and the one with high content of Al_2O_3 (3.8 at%). Therefore, the observed structural changes should be correlated with both increasing Nb and Al contents which have an opposite effect on the structure of the glass; the first one increases the polymerization, and the second one led to depolymerization of phosphate structure.

To analyze the influence of Mg substitution by Nb, now we compare the FTIR spectra of glasses 3.4Nb and 1.4Nb, which contain a small amount of Al_2O_3. In sample 3.4Nb the clear separation of two bands at ~1160 and 1100 cm^{-1} occurred as well as the increase in relative intensity of the highest-frequency band. Moreover, the relative intensity of the band at ~910 cm^{-1} is significantly higher and of the band at 550 cm^{-1} is slightly lower. The band at 997 cm^{-1} is not detectable in sample 3.4Nb. All these changes suggest a more polymerized phosphate network consisting mostly of Q^1 and Q^2 units.

The FTIR spectrum of sample 1.8Nb containing 2.7 at% of Al is close to the ones of 0.8Nb and 0Nb. However, in this sample, the Nb_2O_5 presence is visible in the band at 635 cm^{-1}. Two maxima can be distinguished at 1128 and 1064 cm^{-1} which is also an effect of Nb doping, but the movement of bands into lower frequencies suggests a more depolymerized structure than in samples 3.4Nb and 1.4Nb. The presence of Q^2 units is also visible as a small band at 495 cm^{-1}. Additionally, the relative intensity of bands at 914 cm^{-1} and 560 cm^{-1} are the lowest from all samples spectra. Considering the degree of network polymerization estimated based on FTIR results we can order samples from the highest to the lowest one: 3.4Nb (3.2) > 1.4Nb (3.3) > 1.8Nb (3.5) > 0.8Nb (3.7) > 0Nb (3.7). It is in good agreement with the O:(*P*+Nb) ratios calculated for all samples and listed in brackets. However, at the same time, the order also follows the Al_2O_3 amount in

Table 2
The mass loss of glasses after immersion in PBS for 7 and 14 days.

Step of immersion	Immersion time (days)	Samples code				
		0Nb	0.8Nb	1.4Nb	1.8Nb	3.4Nb
		Mass loss after immersion in PBS (%) ± 0.01				
Initial stage	7	0.08	0.01	0.27	0.02	1.24
Long term	14	2.04	2.10	0.30	0.05	1.52

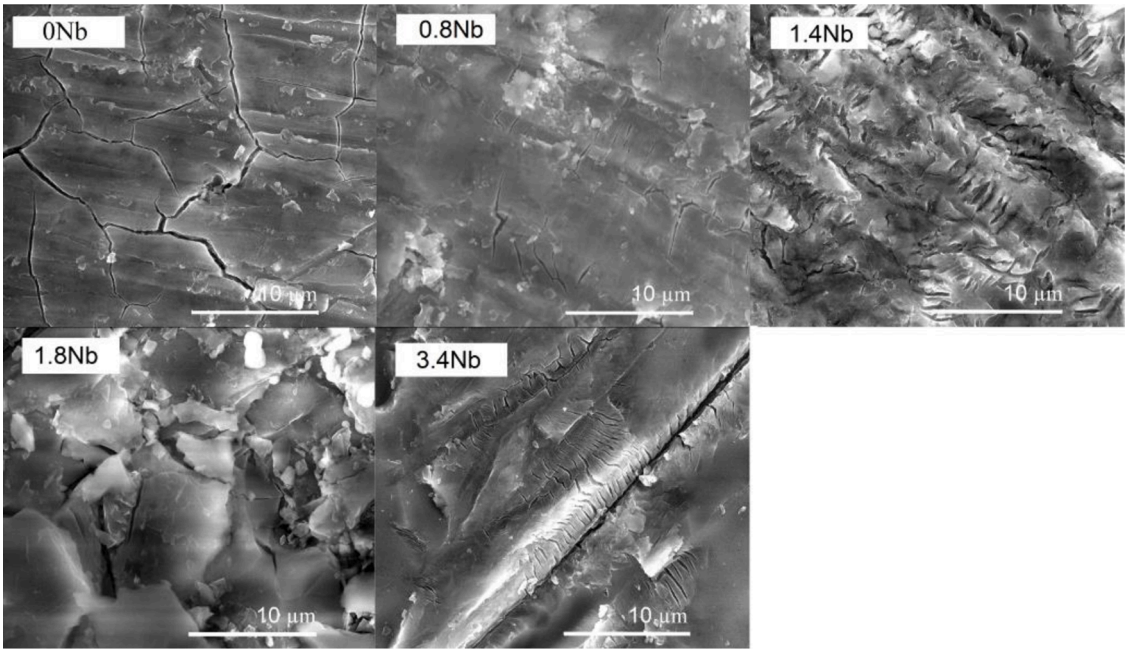

Fig. 4. SEM micrographs after 7 days of immersion in PBS 0Nb, 0.8Nb, 1.4Nb, 1.8Nb and 3.4Nb.

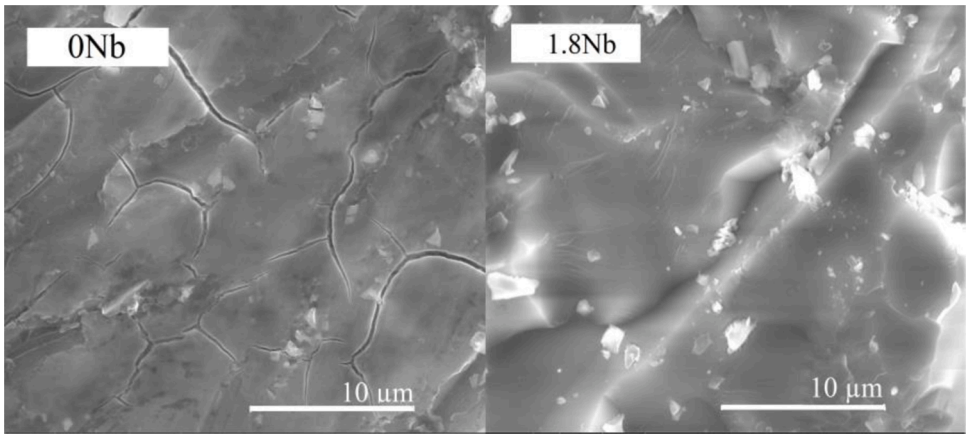

Fig. 5. SEM micrographs after 14 days of incubation in PBS for (left) 0Nb and (right) 1.8Nb.

compositions and confirms its high impact on glass structure. It should be also noted that in Nb-doped glasses the band at ~550 cm^{-1} can be also assigned to the vibrational coupling of [$_{\nu}$(Nb-O) (medium Nb-O distances) (O-P-O)] stretching with deformation modes [33] however no correlation was found between Nb content and its intensity.

3.2. *In vitro* dissolution in PBS

The *in vitro* dissolution tests were carried out in PBS for 7 and 14 days and obtained results are listed in Table 2. The mass loss after the initial stage of dissolution was found to be the highest for sample 3.4Nb having the lowest content of Al. Sample 1.4Nb having 0.8 at% of Mg and less than 2 at% Nb shows 4.5 times lower mass loss than sample 3.4Nb. However, it still shows significantly higher mass loss than other samples containing a high amount of Al_2O_3. Sample 0Nb having a higher amount Al and undoped with Nb exhibits higher mass loss than sample 1.8Nb with lower content of Al (1.1 at%) and doped with Nb (1.8 at%). It suggests that at the initial stage the dissolution process is supported by separate Nb or Mg presence while it is highly suppressed by a high content of Al. During long-term immersion, the dissolution behavior of samples is significantly different. The highest mass loss is observed for two samples containing the highest amount of Al and Mg; 0Nb and 0.8Nb, respectively. While the other samples show only slight progress in the dissolution. To find the possible explanation, the surfaces of samples were analyzed by SEM-EDS in search of the presence of phosphate-based layers. SEM micrographs of the surfaces of all samples after 7 days of immersion in PBS are shown in Fig. 4. On each sample, a phosphates layer was found. However, the thickness of layers was too low to confirm their exact compositions by EDX measurements Fig. 5. presents the layers, which occurred on the surfaces of samples 0Nb and 1.8Nb after 14 days of immersion. In the other samples 1.4Nb, 1.8Nb, and 3.4Nb besides the layer a high content of NaCl crystals was also detected. Its presence may explain the lower loss mass in these samples.

The ion dissolution profiles of Ca, P, Na, Nb, and Mg are displayed in Fig. 6. It can be seen that total P ion content in PBS increases for all samples. During the first 7 days, its increasing rate in PBS is similar for all samples however, after 14 days small differences can be noticed. The long-term releasing of P ion is slower in two samples doped with the highest content of Nb. Ca ion concentration increased in PBS after 7 days of samples immersion. However, after long-term incubation, the total Ca

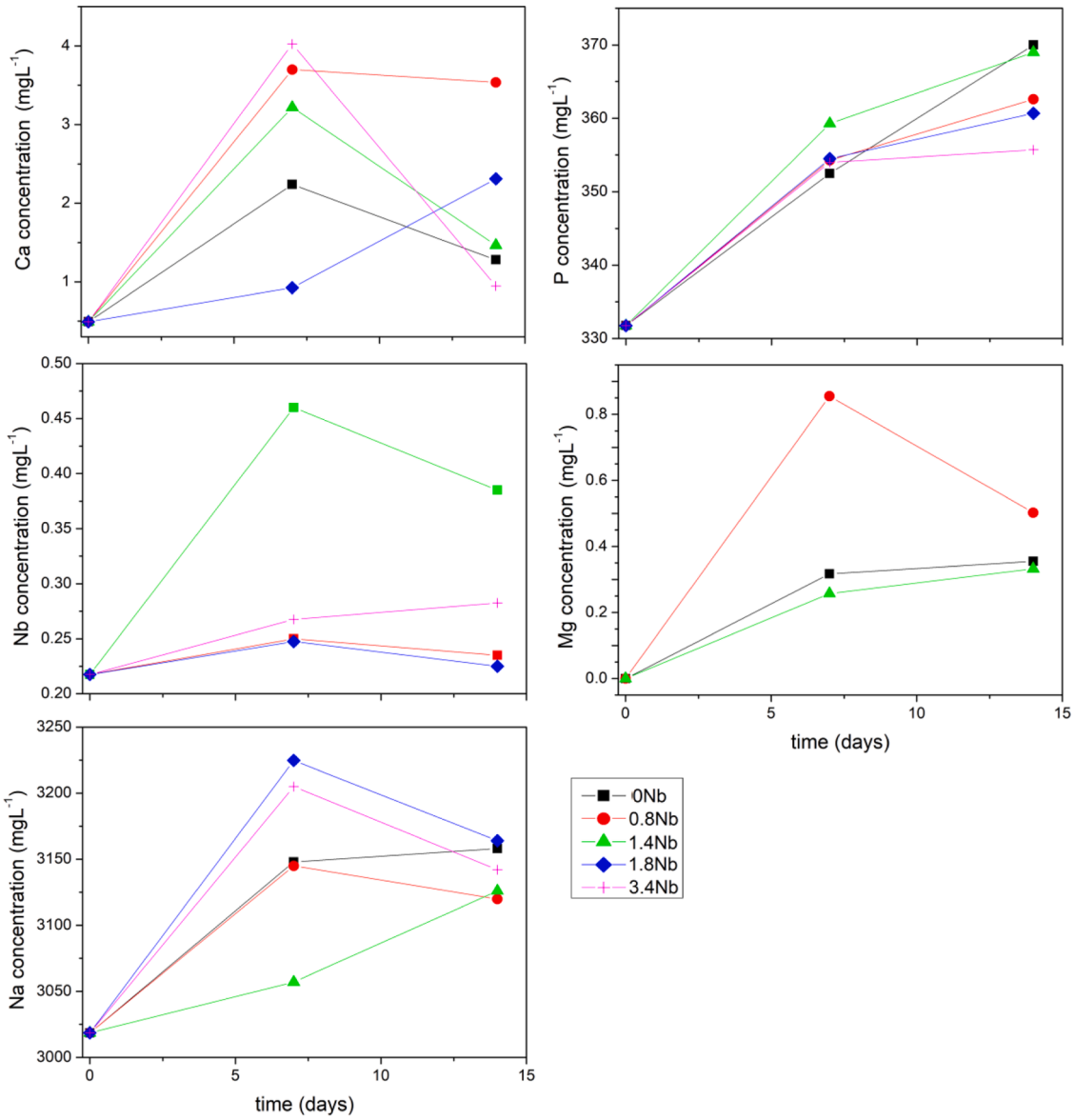

Fig. 6. The ion dissolution profiles of all samples in PBS as a function of immersion time. The experimental errors are smaller than the size of the symbols.

content decreased for most of the samples suggesting the possible transfer of Ca ions to the samples' surfaces. The highest changes in Ca^{2+} behavior are observed for glasses 3.4Nb and 1.4Nb having the lowest content of Al_2O_3. However, also in sample 0Nb undoped with Nb_2O_5 and with quite high content of Al_2O_3 the deposition of Ca^{2+} is supposed. The Na ion concentration in PBS is very high and for most samples, it mostly increases. The behavior of Nb dissolution profiles is different for samples containing high and low content of Al_2O_3. It suggests that the presence of high Al content in glass inhibits the Nb from getting out of the phosphate structure. On the other hand, the small content of Al in sample 3.4Nb (doped only with Nb) did not influence much the slow and constant Nb releasing process into PBS during all immersion time. There is a noticeable Mg supporting effect on Nb escaping from the phosphate structure visible in sample 1.4Nb when the Al content is negligible. The similar importance of Al for Mg releasing is not observed. The Mg^{2+} releases continuously from samples 0Nb and 1.4Nb during all immersion time. A significantly higher total Mg concentration was found in PBS after 7 days of immersion for the sample 0.8Nb. Moreover, the Mg was not detected in PBS after incubation of sample 1.8Nb while no Al was found in any solution after 7 as well as 14 days tests. It suggests that the Al stays highly bonded within the phosphate network in all samples regardless of the content.

To take a higher insight into the *in vitro* dissolution process, which proceeded in PBS, the pH of solutions was checked regularly during immersion time and is displayed in Fig. 7 for all samples. It can be seen that the pH of solutions decreases during the first 7 days or 8 days (for sample 3.4Nb) of immersion and next it slightly increases. During long-term immersion, the pH value stabilizes in all cases and varies between 7.32 and 7.30. The highest changes in pH are found for samples 1.4Nb and 3.4Nb while the lowest for sample 0Nb, however, the differences are only 0.02. The decrease in pH of solutions is a consequence of the dissociation of hydrated phosphate chains [23]. The P–O–P bonds break up due to continuous attack of water and the $[PO_4]$ units are released from the glass network as confirmed by P ion dissolution profiles. The phosphorous cations tend to bond with protons and form phosphoric acid which decreases the pH of the solution [44]. However, the *in vitro* dissolution process of the sodium-calcium-phosphate glasses with short-chain structure consists also of the hydration process during which a hydrated layer is formed on the glass surface as a result of Na^+ and H^+ ion-exchange [44]. The release of Na^+ into solution increases its pH as well as the dissolution of Ca^{2+} and Mg^{2+} as they chelate with the released phosphate species [44]. Therefore, as the dissolution is a

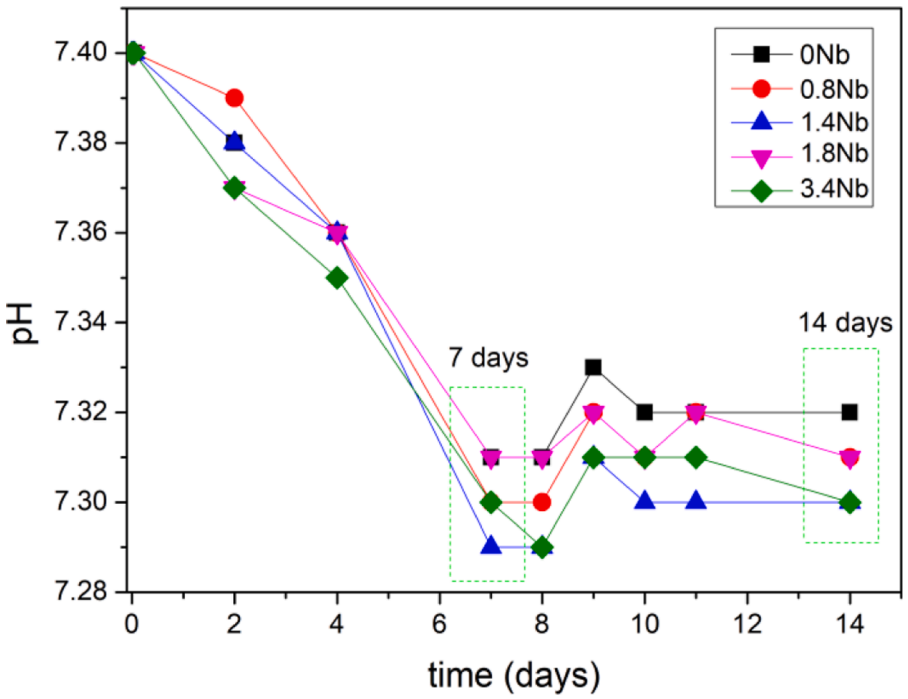

Fig. 7. The pH of PBS as a function of immersion time for all glasses. The experimental errors are smaller than the size of the symbols.

combination of chain hydration and hydrolysis it does not affect the pH that much (change of only 0.1). However, comparing the pH changes observed after immersion of all tested samples it may be presumed that the high content of Al only slightly reduced the reactivity between glasses and solution while Nb presence increased it.

3.3. Thermal properties

In our previous papers [6,45] we have demonstrated the approximately linear correlation between T_g and effective cation field strength (ECFS) found for phospho-silicate and silicate glasses. Similar behavior is expected in phosphate-based glasses. The cation field strengths (CFS) of the modifier ions were calculated using CFS = Z/r^2 where "Z" is the valence of the respective cation and "r" the Shannon-Prewitt ionic radius for eight-coordinated Na, seven-coordinated Ca, six-coordinated Mg, Al, and Nb which is 0.718, 1.780, 3.856, 6.584, 8.218 $Å^{-2}$ for Na^+, Ca^{2+}, Mg^{2+}, Al^{3+}, Nb^{5+}, respectively (see Table 1). In Fig. 8a the T_g is presented as a function of calculated ECFS. The increase in T_g with the ECFS is visible. The Nb addition increases the T_g of phosphate base glasses, due to the increase of network polymerization by Nb addition. However, Al_2O_3 addition was found also to advance the T_g of phosphate glasses while it was shown to suppress the polymerization of structure. It is due to the fact that the formation of the P–O–Al–O–P bridging bonds provides strong cross-linking between phosphate chains [42] as mentioned earlier. Therefore, the T_g behavior considered as a function of sum Al +Nb (see the inset in Fig. 8a) showed an increasing correlation.

Thermal stability can be estimated in two ways: $S_1 = T_{cr1} - T_g$ and $S_2 = T_{cr2} - T_g$ where T_{cr1} is the beginning of the crystallization process (observed at the DSC curve as an exothermic process) and T_{cr2} is the maximum of the crystallization process. In Fig. 8b the glass thermal stabilities are presented as a function of Nb content. A clear increasing trend is noticed with the Nb incorporation. The incorporation of 0.8 at% of Nb increased the glass thermal stability up to 30 °C while the full substitution of MgO by Nb_2O_5 increased it by more than 50 °C. Comparing the samples 1.4Nb and 3.4Nb, it can be stated that the further increasing the Nb content of 2 at%, *S* increased for more than 10 °C, while T_g *for* ~ 40 °C, respectively. It suggests that Nb incorporation suppresses the crystallization process while Mg supports it. These observations are in accord with our previous studies for phosphate glasses [5] and silicate glasses [6].

The liquid fragility index can be obtained from the glass transition width ΔT_g and the jump in heat capacity during the glass transition ΔC_p [46,47]. The $\Delta T_g = T_{g\ offset} - T_{g\ onset}$, where $T_{g\ offset}$ is the offset temperature of the C_p overshoot in the glass transition zone. $\Delta C_p = IC_{pl} - C_{pg}I$, where C_{pg} and C_{pl} are the isobaric heat capacities for the glass at T_g and the liquid, respectively (see [7] for details). It is known that the fragility of liquid is directly proportional to ΔC_p and inversely proportional to ΔT_g, therefore fragility index *m* can be estimated by $m = \Delta C_p \Delta T_g^{-1}$ [48]. An interesting correlation was observed between the glasses *m* values and the ratio O:(P+Al) in which both the degree of polymerization of phosphate network and the influence of Al incorporation is taken into account (see the inset in Fig. 8b). It can be seen that the higher is the content of P and Al, the higher is fragility index of glass. Furthermore, no correlation was found between fragility and Nb content or ECFS.

4. Conclusions

In summary, we have prepared potential bioactive glasses in the Na-Mg-Ca-Nb-Al-P-O system containing different contents of niobium, magnesium, and aluminum. All obtained samples were amorphous and a difference in color was found due to the niobium content. The degree of network depolymerization estimated based on the O:(P+Nb) ratio was in accordance with the FTIR results. The phosphate structure was highly disrupted in all glasses and mostly consists of Q^1 units. However, glasses containing high contents of Mg and Al, contain also short isolated orthophosphate units (Q^0). Nb doping affected in increasing polymerization of glass network, visible as the presence of Q^2 units. Thermal properties analysis showed that Al and Nb contents control the glass transition temperature while glass thermal stability was highly correlated only with the Nb content. No relation between glass fragility and Nb content was observed.

The *in vitro* dissolution test in PBS showed that all glasses exhibit the potential bioactive character and the formation of calcium phosphate layer formed on their surfaces. The pH changes and ion dissolution profiles confirmed that the dissolution of tested samples consists of two processes: the releasing of the [PO_4] units into PBS and the hydration

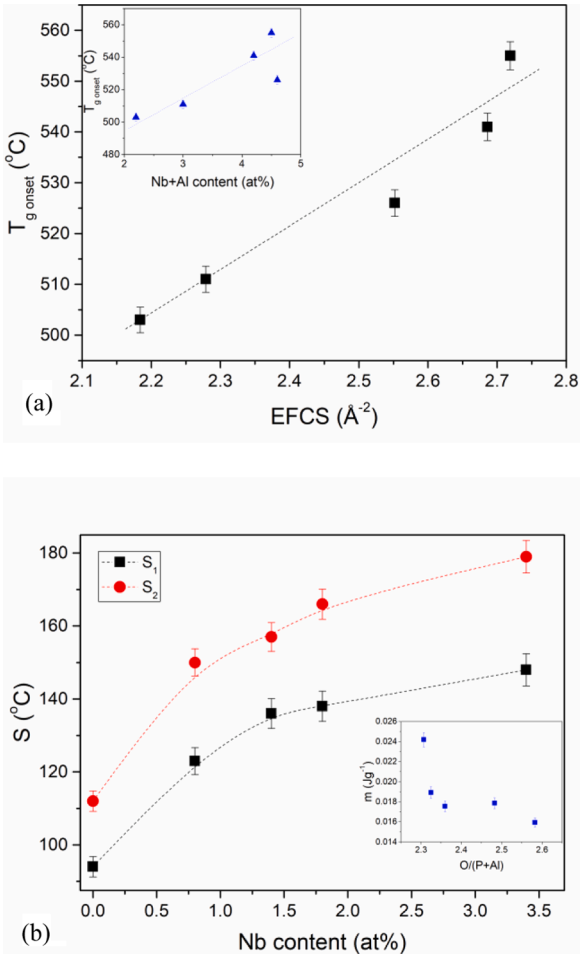

Fig. 8. (a) T_g as a function of ECFS and in inset T_g is function of Al and Nb content. (b) Glass thermal stability as a function of Nb content. Inset in fig. b shows the behavior of index fragility *versus* polymerization of glass network. The dashed lines are a guide for the eye.

process. The high content of Al in samples slightly reduced the Nb releasing while Mg advanced it. No impact of Al is observed for Mg^{2+} releasing. Moreover, the Al^{3+} stays bonded in the phosphate network and does not release into PBS even during long-term immersion. The method and compositions presented in this work could be used as a promising material for the stimulation of bone regeneration.

Data availability

The data that support the findings of this study are available from the corresponding author upon reasonable request.

CRediT authorship contribution statement

Natalia Anna Wójcik: Conceptualization, Data curation, Formal analysis, Funding acquisition, Investigation, Methodology, Project administration, Supervision, Writing – original draft. **Stefania Wolff:** Investigation, Methodology. **Jakub Lech Karczewski:** Methodology, Writing – review & editing. **Małgorzata Rutkowska:** Investigation, Methodology, Writing – review & editing. **Sharafat Ali:** Investigation, Methodology, Writing – review & editing.

Declaration of Competing Interest

The authors declare that they have no known competing financial interests or personal relationships that could have appeared to influence the work reported in this paper.

Acknowledgements

This work was supported by the Gdańsk University of Technology [Grant Number DEC-19/2020/IDUB/I.3.3] under the ARGENTUM TRIGGERING RESEARCH GRANTS - 'Excellence Initiative - Research University' program.

References

[1] J.R. Jones, P. Sepulveda, L.L. Hench, Dose-dependent behavior of bioactive glass dissolution, J. Biomed. Mater. Res. 58 (6) (2001) 720–726, https://doi.org/10.1002/jbm.10053.
[2] D. Ehrt, P. Ebeling, U. Natura, UV Transmission and radiation-induced defects in phosphate and fluoride–phosphate glasses, J. Non. Cryst. Solids 263-264 (2000) 240–250, https://doi.org/10.1016/S0022-3093(99)00681-X.
[3] D. Ehrt, REVIEW: phosphate and fluoride phosphate optical glasses – properties, structure and applications, Phys. Chem. Glass. Eur. J. Glass Sci. Technol. Part B 56 (6) (2015) 217–234, https://doi.org/10.13036/17533562.56.6.217.
[4] E.A. Abou Neel, D.M. Pickup, S.P. Valappil, R.J. Newport, J.C. Knowles, Bioactive functional materials: a perspective on phosphate-based glasses, J. Mater. Chem. 19 (6) (2009) 690. -70, doi:110.1039/b810675d.
[5] N.A. Wójcik, S. Ali, J.L. Karczewski, B. Jonson, M. Bartmański, R.J. Barczyński, DC and AC Conductivity, Biosolubility and thermal properties of Mg-Doped Na_2O–CaO–P_2O_5 glasses, Materials 14 (10) (2021) 2626, https://doi.org/10.3390/ma14102626 (Basel).
[6] N.A. Wójcik, S. Ali, A. Mielewczyk-Gryń, B. Jonson, Two-step synthesis of niobium doped Na–Ca–(Mg)–P–Si–O glasses, J. Mater. Sci. 56 (2021) 7613–7625, https://doi.org/10.1007/s10853-021-05781-w.
[7] N.A. Wójcik, B. Jonson, D. Möncke, D. Palles, E.I. Kamitsos, E. Ghassemali, S. Seifeddine, M. Eriksson, S. Ali, Influence of synthesis conditions on glass formation, structure and thermal properties in the Na_2O-CaO-P_2O_5 system doped with Si_3N_4 and Mg, J. Non. Cryst. Solids 494 (2018) 66–77, https://doi.org/10.1016/j.jnoncrysol.2018.04.055.
[8] H. Maeda, T. Miyajima, S. Lee, A. Obata, K. Ueda, T. Narushima, T. Kasuga, Preparation of calcium pyrophosphate glass-ceramics containing Nb_2O_5, J. Ceram. Soc. Jpn. 122 (2014) 122–124, https://doi.org/10.2109/jcersj2.122.122.
[9] N.A. Wójcik, S. Ali, E.I. Kamitsos, D. Möncke, Niobate in silicate and phosphate glasses: effect of glass basicity on crucible dissolution, Int. J. Appl. Glass Sci. 13 (10) (2022) 121–134, https://doi.org/10.1111/ijag.16505.
[10] L. Petit, T. Cardinal, J.J. Videau, E. Durand, L. Canioni, M. Martines, Y. Guyot, G. Boulon, Effect of niobium oxide introduction on erbium luminescence in borophosphate glasses, Opt Mater (Amst) 28 (3) (2006) 172–180, https://doi.org/10.1016/j.optmat.2004.12.007.
[11] A. Yamamoto, R. Honma, M. Sumita, Cytotoxicity evaluation of 43 metal salts using murine fibroblasts and osteoblastic cells, J. Biomed. Mater. Res. 39 (2) (1998) 331–340, doi:10.1002/(SICI)1097-4636(199802)39:2<331::AID−JBM22>3.0.CO;2-E.
[12] L.P.L. de Souza, J.H. Lopes, F.V. Ferreira, R.A. Martin, C.A. Bertran, J.A. Camilli, Evaluation of effectiveness of 45S5 bioglass doped with niobium for repairing critical-sized bone defect in *in vitro* and *in vivo* models, J. Biomed. Mater. Res. Part A 108 (3) (2020) 446–457, https://doi.org/10.1002/jbm.a.36826.
[13] L. Souza, J.H. Lopes, D. Encarnação, I.O. Mazali, R.A. Martin, J.A. Camilli, C. A. Bertran, Comprehensive *in vitro* and *in vivo* studies of novel melt-derived Nb-substituted 45S5 bioglass reveal its enhanced bioactive properties for bone healing, Sci. Rep. 8 (1) (2018) 12808, https://doi.org/10.1038/s41598-018-31114-0.
[14] A. Obata, Y. Takahashi, T. Miyajima, K. Ueda, T. Narushima, T. Kasuga, Effects of niobium ions released from calcium phosphate invert glasses containing Nb_2O_5 on osteoblast-like cell functions, ACS Appl. Mater. Interfaces 4 (10) (2012) 5684–5690, https://doi.org/10.1021/am301614a.
[15] V. Miguez-Pacheco, D. de Ligny, J. Schmidt, R. Detsch, A.R. Boccaccini, Development and characterization of niobium-releasing silicate bioactive glasses for tissue engineering applications, J. Eur. Ceram. Soc. 38 (3) (2018) 871–876, https://doi.org/10.1016/j.jeurceramsoc.2017.07.028.
[16] M. Silva, C. Ramirez, J. Granjeiro, A. Rossi, *In vitro* assessment of new niobium phosphate glasses and glass ceramics, Key Eng. Mater. 361–363 (I) (2008) 229–232. KEY ENG MAT10.4028/.
[17] D. Möncke, E.I. Kamitsos, D. Palles, R. Limbach, A. Winterstein-Beckmann, T. Honma, Z. Yao, T. Rouxel, L. Wondraczek, Transition and post-transition metal ions in borate glasses: borate ligand speciation, cluster formation, and their effect on glass transition and mechanical properties, J. Chem. Phys. 145 (12) (2016), 124501, https://doi.org/10.1063/1.4962323.
[18] A. Thieme, D. Möncke, R. Limbach, S. Fuhrmann, E.I. Kamitsos, L. Wondraczek, Structure and properties of alkali and silver sulfophosphate glasses, J. Non Cryst. Solids 410 (0) (2015) 142–150, https://doi.org/10.1016/j.jnoncrysol.2014.11.029.
[19] K. Griebenow, C.B. Bragatto, E.I. Kamitsos, L. Wondraczek, Mixed-modifier effect in alkaline earth metaphosphate glasses, J. Non Cryst. Solids 481 (2018) 447–456, https://doi.org/10.1016/j.jnoncrysol.2017.11.041.
[20] A. Sharafat, J. Grins, S. Esmaeilzadeh, Properties of high nitrogen content mixed alkali earth oxynitride glasses $(AE_xCa_{1-x})_{1.2(1)}SiO_{1.9(1)}N_{0.86(6)}$, AE=Mg, Sr, Ba,

J. Non Cryst. Solids 355 (22–23) (2009) 1259–1263, https://doi.org/10.1016/j.jnoncrysol.2009.04.036.
[21] S. Ali, B. Jonson, Compositional effects on the properties of high nitrogen content alkaline-earth silicon oxynitride glasses, AE=Mg, Ca, Sr, Ba, J. Eur. Ceram. Soc. 31 (4) (2011) 611–618, https://doi.org/10.1016/j.jeurceramsoc.2010.11.005.
[22] S. Ali, B. Jonson, M.J. Pomeroy, S. Hampshire, Issues associated with the development of transparent oxynitride glasses, Ceram. Int. 41 (3, Part A) (2015) 3345–3354, https://doi.org/10.1016/j.ceramint.2014.11.030.
[23] I.H. Lee, S.H. Shin, F. Foroutan, N.J. Lakhkar, M.S. Gong, J.C. Knowles, Effects of magnesium content on the physical, chemical and degradation properties in a $MgO-CaO-Na_2O-P_2O_5$ glass system, J. Non Cryst. Solids 363 (2013) 57–63, https://doi.org/10.1016/j.jnoncrysol.2012.11.036.
[24] A.A. El-Kheshen, F.A. Khaliafa, E.A. Saad, R.L. Elwan, Effect of Al_2O_3 addition on bioactivity, thermal and mechanical properties of some bioactive glasses, Ceram. Int. 34 (7) (2008) 1667–1673, https://doi.org/10.1016/j.ceramint.2007.05.016.
[25] K.S.T. Manupriya, K. Singh, G. Sharma, V. Rajendran, Influence of addition of Al_2O_3 on physical, structural, acoustical and in-vitro bioactive properties of phosphate glasses, Phys. Status Solidi (a) 206 (7) (2009) 1447–1455, https://doi.org/10.1002/pssa.200824426.
[26] J. Smith, S. King, E. Barney, J. Hanna, R. Newport, D. Pickup, Structural study of Al_2O_3-Na_2O-CaO-P_2O_5 bioactive glasses as a function of aluminium content, J. Chem. Phys. 138 (2013), https://doi.org/10.1063/1.4774330.
[27] C. Ohtsuki, T. Kokubo, T. Yamauro, Compositional dependence of bioactivity of glasses in the system CaO-SiO_2-Al_2O_3: it*sin vitro* evaluation, J. Mater. Sci. Mater. Med. 3 (2) (1992) 119–125, https://doi.org/10.1007/BF00705279.
[28] A. Kiani, J.V. Hanna, S.P. King, G.J. Rees, M.E. Smith, N. Roohpour, V. Salih, J. C. Knowles, Structural characterization and physical properties of P_2O_5-CaO-Na_2O-TiO_2 glasses by Fourier transform infrared, Raman and solid-state magic angle spinning nuclear magnetic resonance spectroscopies, Acta Biomater. 8 (1) (2012) 333–340, https://doi.org/10.1016/j.actbio.2011.08.025.
[29] Y.M. Moustafa, K. El-Egili, Infrared spectra of sodium phosphate glasses, J. Non Cryst. Solids 240 (1–3) (1998) 144–153, https://doi.org/10.1016/S0022-3093(98)00711-X.
[30] D. Carta, D.M. Pickup, J.C. Knowles, I. Ahmed, M.E. Smith, R.J. Newport, A structural study of sol-gel and melt-quenched phosphate-based glasses, J. Non Cryst. Solids 353 (18–21) (2007) 1759–1765, https://doi.org/10.1016/j.jnoncrysol.2007.02.008.
[31] P.Y. Shih, Properties and FTIR spectra of lead phosphate glasses for nuclear waste immobilization, Mater. Chem. Phys. 80 (1) (2003) 299–304, https://doi.org/10.1016/S0254-0584(02)00516-3.
[32] I. Konidakis, C.P.E. Varsamis, E.I. Kamitsos, D. Moncke, D. Ehrt, Structure and properties of mixed strontium-manganese metaphosphate glasses, J. Phys. Chem. C 114 (19) (2010) 9125–9138, https://doi.org/10.1021/jp101750t.
[33] S. Lee, T. Nakano, T. Kasuga, Structure, dissolution behavior, cytocompatibility, and antibacterial activity of silver-containing calcium phosphate invert glasses, J. Biomed. Mater. Res. Part A 105 (11) (2017) 3127–3135, https://doi.org/10.1002/jbm.a.36173.
[34] R. Scholz, R.L. Frost, Y.F. Xi, L.M. Graca, L. Lagoeiro, A. Lopez, Vibrational spectroscopic characterization of the phosphate mineral phosphophyllite - $Zn_2Fe(PO_4)(_2)$center dot $4H(_2)O$, from Hagendorf Sud, Germany and in comparison with other zinc phosphates, J. Mol. Struct. 1039 (2013) 22–27, https://doi.org/10.1016/j.molstruc.2013.01.075.
[35] C.Y. Kim, A.E. Clark, L.L. Hench, Early stages of calcium-phosphate layer formation in bioglasses, J. Non Cryst. Solids 113 (2–3) (1989) 195–202, https://doi.org/10.1016/0022-3093(89)90011-2.
[36] M. Dussauze, E.I. Kamitsos, E. Fargin, V. Rodriguez, Structural rearrangements and second-order optical response in the space charge layer of thermally poled sodium-niobium borophosphate glasses, J. Phys. Chem. C 111 (39) (2007) 14560–14566, https://doi.org/10.1021/jp074335f.
[37] R.K. Brow, Review: the structure of simple phosphate glasses, J. Non Cryst. Solids 263 (1–4) (2000) 1–28, https://doi.org/10.1016/S0022-3093(99)00620-1.
[38] G. Walter, J. Vogel, U. Hoppe, P. Hartmann, The structure of $CaO–Na_2O–MgO–P_2O_5$ invert glass, J. Non Cryst. Solids 296 (3) (2001) 212–223, https://doi.org/10.1016/S0022-3093(01)00912-7.
[39] M. Dussauze, E. Kamitsos, F. Evelyne, V. Rodriguez, Structural rearrangements and second-order optical response in the space charge layer of thermally poled sodium−niobium borophosphate glasses, J. Phys. Chem. C 111 (2007) 14560–14566, https://doi.org/10.1021/jp074335f.
[40] N.A. Wójcik, N.S. Tagiara, S. Ali, K. Górnicka, H. Segawa, T. Klimczuk, B. Jonson, D. Möncke, E.I. Kamitsos, Structure and magnetic properties of BeO-Fe_2O_3-Al_2O_3-TeO_2 glass-ceramic composites, J. Eur. Ceram. Soc. 41 (2021) 5214–5222, https://doi.org/10.1016/j.jeurceramsoc.2021.04.005.
[41] N.A. Wójcik, S. Ali, D. Möncke, N.S. Tagiara, E.I. Kamitsos, H. Segawa, M. Eriksson, B. Jonson, The influence of Be addition on the structure and thermal properties of alkali-silicate glasses, J. Non Cryst. Solids 521 (2019), 119532, https://doi.org/10.1016/j.jnoncrysol.2019.119532.
[42] I. Konidakis, C.P.E. Varsamis, E.I. Kamitsos, Effect of synthesis method on the structure and properties of $AgPO_3$-based glasses, J. Non Cryst. Solids 357 (14) (2011) 2684–2689, https://doi.org/10.1016/j.jnoncrysol.2011.03.013.
[43] Z.C.Y. Er-rouissi, N. Beloued, S. Aqdim, Chemical durability and structural properties of Al_2O_3-CaO-Na_2O-P_2O_5 glasses studied by IR spectroscopy, XRD and SEM, Adv. Mater. Phys. Chem. 7 (2017) 353–363, https://doi.org/10.4236/ampc.2017.710028.
[44] E. El-Meliegy, M.M. Farag, J.C. Knowles, Dissolution and drug release profiles of phosphate glasses doped with high valency oxides, J. Mater. Sci. Mater. Med. 27 (6) (2016), 10810.1007/s10856-016-5711-8.
[45] S. Ali, N.A. Wójcik, B. Jonson, E.I. Kamitsos, X. Li, J. Luo, D. Möncke, Synthesis, structural characterization, and thermal properties of Ca- and La-doped soda-lime glasses by laser melting, Int. J. Appl. Glass Sci. 11 (2020) 699–706, https://doi.org/10.1111/ijag.15477.
[46] G.L. Paraschiv, F. Muñoz, L.R. Jensen, Y. Yue, M.M. Smedskjaer, Impact of nitridation of metaphosphate glasses on liquid fragility, J. Non Cryst. Solids 441 (2016) 22–28, https://doi.org/10.1016/j.jnoncrysol.2016.03.009.
[47] G.L. Paraschiv, F. Muñoz, G. Tricot, N. Mascaraque, L.R. Jensen, Y. Yue, M. M. Smedskjaer, Mixed alkali silicophosphate oxynitride glasses: structure-property relations, J. Non Cryst. Solids 462 (2017) 51–64, https://doi.org/10.1016/j.jnoncrysol.2017.02.011.
[48] G.D. Chryssikos, J.A. Duffy, J.M. Hutchinson, M.D. Ingram, E.I. Kamitsos, A. J. Pappin, Lithium borate glasses - a quantitative study of strength and fragility, J. Non Cryst. Solids 172 (1994) 378–383, https://doi.org/10.1016/0022-3093(94)90460-X.